with a pH of 7.4. Currents were recorded with an Axopatch 200 (Axon Instruments, Foster City, CA) with 70 to 90% compensation of the 10 to 50-megohm series resistance. In each slice, we recorded the responses of at least one control cell. In experiments in which muscimol was applied, each cell perfused with CsF-DIDS was tested with puffs applied at three or more different locations near the recording electrode. Synaptic currents were evoked at a frequency of 0.2 Hz by means of bipolar electrodes placed near the recording site. Stimulus intensity (0.1 to 1.5 mA for 0.1 ms) was adjusted to yield maximal responses.

12. Electrically evoked inhibitory currents contained a large monosynaptic component that persisted in control cells (n = 5) during a bath application of 10 μM 6-cyano-7-nitroquinoxaline-2,3-dione (CNQx) and 30 μM D,L-2-amino-5-phosphonovaleric acid (APV). The time course and voltage dependence of the early and late components of the synaptic response of cells perfused with CsF-DIDS closely resembled those of the two components of excitatory postsynaptic currents (EPSCs) previously described in hippocampal [S. Hestrin, R. A. Nicoll, D. J. Perkel, P. Sah, *J. Physiol. (London)* **422**, 203 (1990)] and visual cortical neurons [P. Stern, F. A. Edwards, B. Sakmann, *ibid.* **449**, 247 (1992)]. The late component was blocked by 30 μM APV (n = 3). No synaptic response remained when both CNQx and APV were present (n = 2).
13. Anesthesia was initiated with ketamine (30 mg per kilogram of body weight) and xylazine (3 mg/kg), given intramuscularly and maintained with isofluorane (1 to 2%, delivered through a tracheal cannula in a 70:30 mixture of N_2O and O_2). Cats were paralyzed with intravenous gallamine triethiodide (3.6 mg/hour) and artificially respired to maintain end-tidal CO_2 at 3.5%. An animal's electroencephalograph and heart rate were continuously monitored to ensure adequate anesthesia. Bilateral pneumothorax and cisternal drainage were done to improve stability. Techniques for in vivo whole-cell recording and visual and electrical stimulation were similar to those recently described (*3*) [X. Pei, M. Volgushev, T. R. Vidyasagar, O. D. Creutzfeldt, *Neuroreport* **2**, 485 (1991)]. Electrodes (tip size, 2 μm; 4 to 10 megohm resistance) containing control solution (15 cells) or CsF-based solution (see *11*), with added DIDS (0.5 mM, eight cells; 2 mM, six cells) or PTX (1 mM, four cells), were advanced down the medial bank of the lateral gyrus 0 to 5 mm posterior to the interaural line. Cells were encountered at depths of 300 to 2000 μm. Seal resistances were >1 gigohm. In most cases, we mapped extracellular responses using hand-held or computer-driven stimuli and classified cells as simple or complex. Responses were recorded by means of an Axopatch 200 in voltage clamp mode (4 cells) or by an Axoclamp in standard bridge mode (29 cells) and were digitized onto videotape (22 kHz) and onto a 486 computer (1 to 2 kHz). In vivo whole-cell recordings were obtained from 33 neurons in 17 female cats (15 cats aged 8 to 14 weeks and 2 adult cats). Initial membrane potentials were −40 to −71 mV, and input resistances were 80 to 320 megohms. Cells recorded with electrodes containing cesium-based solutions quickly developed depolarized membrane potentials (−10 to −35 mV) and broadened action potentials (duration 10 to 50 ms) lacking afterhyperpolarizations, whereas spontaneous firing increased. For cells recorded with inhibitory blocking solutions, responses used for quantitative comparison were collected at least 15 min after recording began and remained stable for up to 2.5 hours. In most cases, we recorded while applying constant hyperpolarizing current that was sufficient to prevent elevated spontaneous firing.
14. D. Ferster, *J. Neurosci.* **8**, 1172 (1988).
15. B. Jagadeesh, H. S. Wheat, D. Ferster, *Science* **262**, 1901 (1993).
16. A. M. Sillito, *J. Physiol. (London)* **271**, 699 (1977).
17. R. J. Douglas and K. A. C. Martin, *ibid.* **440**, 735 (1991).
18. A. B. Bonds, *Visual Neurosci.* **2**, 41 (1989).
19. E. L. White, *Cortical Circuits* (Birkhäuser, Boston, 1989), p. 69.
20. We have recently found, in detailed simulations of visual cortical circuitry, that disinhibition in single neurons has little effect on their orientation selectivity if constant hyperpolarizing current is applied, but that disinhibition of a group of interconnected excitatory neurons dramatically impairs selectivity without necessarily causing response saturation [D. Somers, S. B. Nelson, M. Sur, *Soc. Neurosci. Abstr.* **19**, 628 (1993)].
21. We thank D. Ferster and B. Connors for helpful suggestions and P. Schiller for comments on the manuscript. Supported by National Eye Institute grants EY06363 and EY07023.

3 February 1994; accepted 13 June 1994

NMR Solution Structure of a Peptide Nucleic Acid Complexed with RNA

Stephen C. Brown,* Stephen A. Thomson, James M. Veal, Donald G. Davis

Peptide nucleic acids (PNA) incorporating nucleic acid bases into an achiral polyamide backbone bind to DNA in a sequence-dependent manner. The structure of a PNA–ribonucleic acid (RNA) complex was determined with nuclear magnetic resonance methods. A hexameric PNA formed a 1:1 complex with a complementary RNA that is an antiparallel, right-handed double helix with Watson-Crick base pairing similar to the "A" form structure of RNA duplexes. The achiral PNA backbone assumed a distinct conformation upon binding that differed from previously proposed models and provides a basis for further structure-based design of antisense agents.

A novel therapeutic strategy is to titrate the concentration of a target enzyme or receptor by altering its expression either at the transcriptional level (antigene) or translational level (antisense) by means of an agent directed against the nucleic acid sequence encoding the target (*1*). Although this approach has been shown to work in mammalian and plant cells (*2*) with the use of natural and modified nucleic acids (*3*), significant obstacles to using such gene-targeted agents to treat human disease remain unsolved (*4*). PNAs incorporating the nucleic acid bases adenine, cytosine, thymine, and guanine into a polyamide backbone have been described (*5*) and are of interest as gene-targeting agents. They are made with standard peptide chemistries fully compatible with automated solid-phase synthesis, bind more tightly to their DNA targets than does the cognate DNA strand, and are sensitive to mismatch (*6*).

We conducted a nuclear magnetic resonance (NMR) investigation to describe the structure of a PNA-RNA complex containing all four common bases. The sequence GAACTC chosen for the PNA (Fig. 1) is capped with G-C base pairs to improve the stability of the complex. The PNA was synthesized with >98% enrichment of ^{13}C and ^{15}N nuclei on the backbone (*7*) of the thymine PNA monomer. In this way, isotope-filtering and isotope-detecting heteronuclear NMR experiments (*8*) could facilitate ^1H resonance assignments and provide more information regarding the structure and dynamics of the PNA backbone.

Titrations of PNA GAACTC-K# (*bis*-succinyl) and r(GAGUUC) followed by NMR indicated only a 1:1 complex formed at all ratios, with six imino resonances appearing from reduced solvent exchange rates (Fig. 2A). NMR spectra of the uncomplexed PNA indicated that many conformers were present in slow chemical exchange (Fig. 2C) because of *cis-trans* equilibria about the secondary amide bond, χ_1, of each PNA residue, whereas in the PNA-RNA complex only one resonance was detected for each proton (Fig. 2B). These data suggest that the PNA backbone adopts a single χ_1 conformation when bound to the complementary RNA strand.

A complete set of two-dimensional (2D) homonuclear NMR data (*9*) provided proton resonance assignments of the PNA-RNA complex by standard methodologies (*10*). The single thymine residue (T_5) was easily identified by both double-quantum (2Q) and total correlation spectroscopy (TOCSY) spectra (*9*). Observation of strong nuclear Overhauser effect (NOE) cross peaks to two adjacent pyrimidine H5,H6 proton pairs identified these as the flanking cytosine bases C_4 and C_6. NOE cross peaks between cytosine H5 and 4-NH_2 resonances were followed to the guanine imino proton, whereas NOEs among the six imino resonances and aro-

Glaxo Research Institute, Research Triangle Park, NC 27709, USA.

*To whom correspondence should be addressed.

Table 1. Conformational parameters for PNA-RNA heteroduplex. The symbols α, β, γ, δ, ε, ζ, χ, χ_1, χ_2, and χ_3 represent either the standard torsional angles (in degrees) describing nucleic acid conformation (*10*) or the torsional angles defined for the PNA structure (both in degrees) in Fig. 1. The pseudorotation value (*P*), and the degree of pucker (τ) are given. Principal values are for the simulated annealing structure with the lowest

	RNA								
Base	α	β	γ	δ	ε	ζ	χ	*P*	τ
G7	—	—	−164 ± 15	81 ± 5	−158 ± 20	−63 ± 10	−163 ± 10	0 ± 10	41 ± 5
A8	−72 ± 5	174 ± 25	66 ± 10	78 ± 5	−148 ± 40	−66 ± 20	−157 ± 20	7 ± 10	39 ± 5
G9	120 ± 15	−166 ± 40	−165 ± 35	91 ± 15	−152 ± 10	−64 ± 5	−174 ± 10	−8 ± 15	38 ± 5
U10	−83 ± 10	−172 ± 20	52 ± 5	76 ± 5	−168 ± 25	−67 ± 10	−165 ± 5	8 ± 11	40 ± 5
U11	−76 ± 10	−176 ± 10	60 ± 5	79 ± 5	−169 ± 17	−67 ± 10	−153 ± 10	13 ± 5	37 ± 5
C12	−77 ± 5	173 ± 10	67 ± 5	73 ± 5	—	—	−148 ± 15	20 ± 25	37 ± 5

matic protons of the bases established their assignments. The intermolecular recognition is standard Watson-Crick for all base pairs: For G-C base pairs, there were strong NOE cross peaks from the cytosine 4 NH_2 to the guanine imino proton; for A-T base pairs, there was a strong NOE from the thymine imino to the H2 of the paired adenine and a weaker NOE to the adenine 6 NH_2. Adenine H2 and H8 resonances were distinguished by the chemical shift of their attached carbon atom, determined by a 2D ^1H-^{13}C heteronuclear multiple quantum coherence (HMQC) experiment (*8*) at natural abundance.

Assignments of RNA backbone resonances proceeded from the base assignments. RNA H1′ resonances were distinguishable by their chemical shifts (5 to 6 ppm), whereas the remaining ribose protons were grouped together (3 to 5 ppm). Scalar couplings from the H1′ to other protons were negligible (<0.5 Hz), so NOE buildup curves were examined and assignments of ribose resonances were made for each RNA residue. Assignments of ribose H3′ and H5′,5″ resonances were verified with ^{31}P-^1H correlation spectra (*8*). Inspection of the NOE network among ribose and base protons revealed that (i) the glycosidic torsion angle is *anti*, not *syn*, for each RNA residue and that (ii) the interresidue and intraresidue NOE patterns are typical of "A" form helices (*10*), with especially strong H2′-H6,H8 sequentials.

Assignments of PNA backbone resonances were more difficult. The standard PNA backbone monomer contains four geminal proton pairs that have nearly degenerate chemical shifts, and no useful homonuclear vicinal scalar couplings exist. However, 2D homonuclear 2Q spectra indicated large chemical shift differences between the diastereotopic protons in all 24 geminal pairs of the six PNA residues. Each of the six PNA backbone amide (NH1′) resonances was resolved, and TOCSY transfer without water presaturation (*11*) established assignments of the NH1′, H2′,H2″ and H3′,H3″ resonances. The G_1 PNA amide was assigned by NOE observations to a succinyl methylene, and a NOE "walk" from the amide to the COOH-terminus permitted the complete assignment of the PNA backbone. NOEs between each backbone amide to intraresidue H3′,H3″ protons and H5′,H5″ protons of the preceding residue were observed, while NOE interactions of H8′,H8″ geminal pairs with base H6,H8 and H3′,H3″ protons established their assignments. Thus, a complete proton resonance assignment of the complex was achieved.

These assignments based on NOE patterns were confirmed with 2D heteronuclear editing or detection experiments (*8*) that focused information on the thymine PNA backbone resonances. Two-dimensional ^{13}C-filtered NOESY experiments were crucial in further identification of the local conformation of the PNA backbone. NOEs were observed from the H8″ proton to the H3′ proton (Fig. 3) but not to the H5′,H5″ protons. NOE interactions between the base H6 or H8 proton and the backbone H8′,H8″ protons were strongly asymmetric in intensity, with the base proton to H8″ interaction being significantly stronger. The NMR data combined with the observation of an overall antiparallel conformation for the PNA-RNA duplex supplied constraints on the conformation of the PNA backbone within a duplex structure.

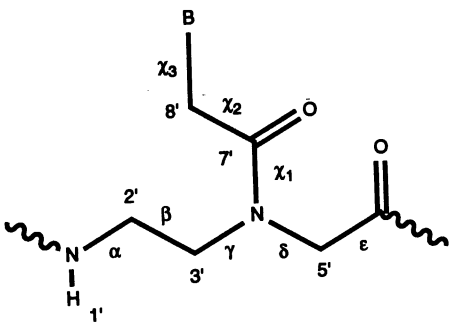

Fig. 1. A PNA structure with atom and torsion-angle labeling convention; B, nucleic acid base. The PNA sequence follows the peptide convention, left-to-right, corresponding to NH_2 to COOH: The PNA(GAACTC)-K#(*bis*-succinyl) sequence was studied. The COOH-terminus was capped with an amidated lysine, and the two free amines were succinylated to improve solubilities (*7*).

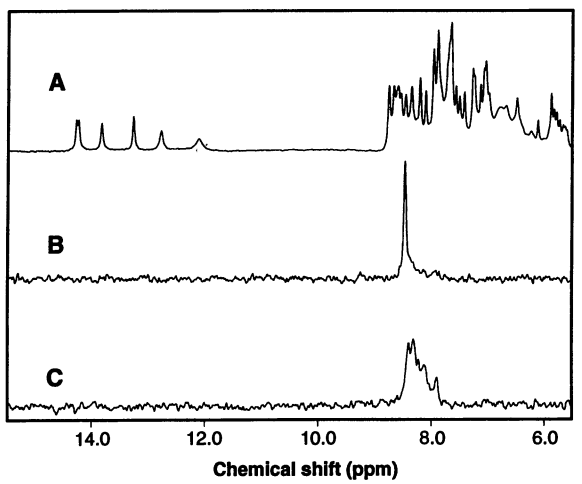

Fig. 2. ^1H-NMR spectra at 25°C of (**A**) jump-and-return of PNA-RNA complex with six imino resonances (12 to 15 ppm) (**B**) ^{15}N-edited spin-echo difference spectrum (*8*) of PNA-RNA complex. The single ^{15}N-labeled PNA amide (T_5) shows a single sharp resonance. (**C**) Uncomplexed PNA, identical conditions and experiment as in (B). The single labeled amide proton displays several resonances in slow exchange, due to *cis-trans* equilibria about the secondary amide (χ_1) of each monomer in the hexameric PNA.

root-mean-square deviation from the average structure of all simulated annealing structures (also the lowest energy structure). The ± ranges reflect deviations observed for other simulated annealing conformations similar to those of the low root-mean-square deviation structure, but do not include alternate conformational values reflecting concerted structural changes (RNA BI to BII; PNA β *gauche*+ to *trans*).

	PNA							
Base	α	β	γ	δ	ε	χ_1	χ_2	χ_3
G1	—	44 ± 20	64 ± 22	78 ± 35	81 ± 35	−2 ± 5	177 ± 10	72 ± 5
A2	169 ± 15	71 ± 15	80 ± 5	72 ± 25	76 ± 25	6 ± 5	−170 ± 25	71 ± 10
A3	172 ± 45	72 ± 20	86 ± 20	74 ± 55	105 ± 180	3 ± 5	−146 ± 35	58 ± 40
C4	150 ± 30	57 ± 10	80 ± 10	76 ± 50	64 ± 105	9 ± 15	−146 ± 30	68 ± 30
T5	170 ± 80	67 ± 10	79 ± 5	85 ± 30	87 ± 20	4 ± 15	−171 ± 35	84 ± 25
C6	157 ± 35	62 ± 15	74 ± 15	—	—	2 ± 5	−175 ± 10	82 ± 30

Initial structures of the PNA-RNA complex were built with the ~150 assigned NOE cross peaks by a distance geometry algorithm and were further refined with simulated annealing protocols (*12*). The overlaid calculated structures show reasonable convergence (Fig. 4). The salient features of these structures, in terms of torsion bond angles and helical properties, are listed in Table 1. The RNA strand adopts a conformation very close to standard "A" form helical geometry (*13*), with ribose pseudorotation angles near 0° and χ angles near −160°. Left-handed helices or structures built with PNA inter-residue *cis* amide bonds did not satisfy the NMR restraints.

The secondary amide of the PNA backbone (Fig. 5A) is exclusively observed as the rotamer with the oxygen of the C7′ carbonyl directed toward the COOH-terminus. The NMR data indicate that the amide protons of the PNA backbone do not participate in internal hydrogen bonds. No protection of the amide proton from chemical exchange with H_2O was observed, chemical shifts are inconsistent with hydrogen bonds, and the simulated annealing-refined structures show long amide hydrogen to carbonyl oxygen distances (on average ≥2.8 Å) and poor N − H − O angles (≈130°) for hydrogen bonding. These results depart from published molecular modeling studies (*14*), where the 7′ carbonyl oxygen participates in a hydrogen bond with the amide proton of the previous PNA residue.

The PNA backbone is not as well restrained by the experimental data as the rest of the structure. PNA backbone resonances are significantly broadened, compared to those of the base protons or the RNA protons, and stereospecific assignments were not possible for any other than the H8′,H8″ geminal pairs. A *gauche* torsion angle in the ethylenediamine region of the backbone (NCCN ≈ +60°) is preferred in the majority of the refined structures, but *trans* torsion angles occur for one or two of the residues in each structure. The line-broadening suggests that this angle is due to conformational flexibility, rather than an artifact due to a lack of experimental restraints. The refined structures presented here indicate significant flexibility about the two dihedral angles immediately flanking the primary amide bond. Such flexibility could be an asset with respect to binding in that periodic fluctuating conformational adjustments could permit the PNA to remain in register with its complementary RNA strand.

Three classes of low-energy conformations (Fig. 5, B to D) were found during modeling studies of PNA-RNA complexes (*15*). One of these models (Fig. 5B) corresponded to that found experimentally (Fig. 5A) and had the lowest calculated energy of the three. Asymmetric NOE intensities between base H6,H8 protons and H8′,H8″ protons rule out one model (Fig. 5C), while the remaining model (Fig. 5D) predicts, within the context of an overall antiparallel conformation, NOEs from H8′,H8″ to H5′,H5″ rather than from H8′,H8″ to H3′,H3″ protons. These modeling studies provided some insight into the basis for the stability of the observed structure. The adop-

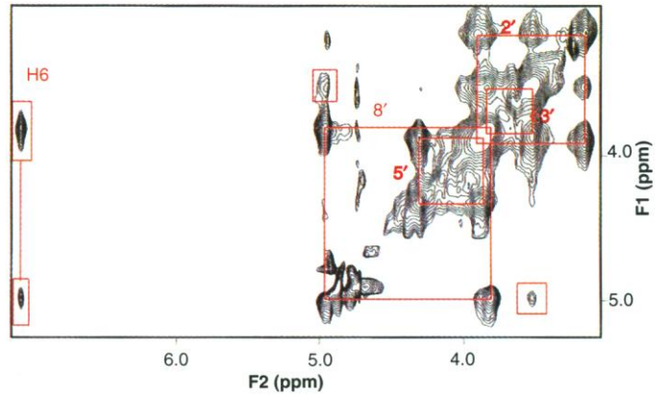

Fig. 3. Two-dimensional NOESY (τ_m = 200 ms), F1 ^{13}C-filtered (*8*) of PNA-RNA complex. Only magnetization originating from protons attached to a labeled ^{13}C is transferred to other nearby protons. Boxes across the diagonal connect the four geminal pairs of labeled residue T_5. Boxes (3.5 and 5.0 ppm) identify NOE cross peaks between the H8′ and H3″ proton establishing orientation of the secondary amide. Note the asymmetry of H8″ and H8′ NOE intensities to the H6 base proton (7.1 ppm).

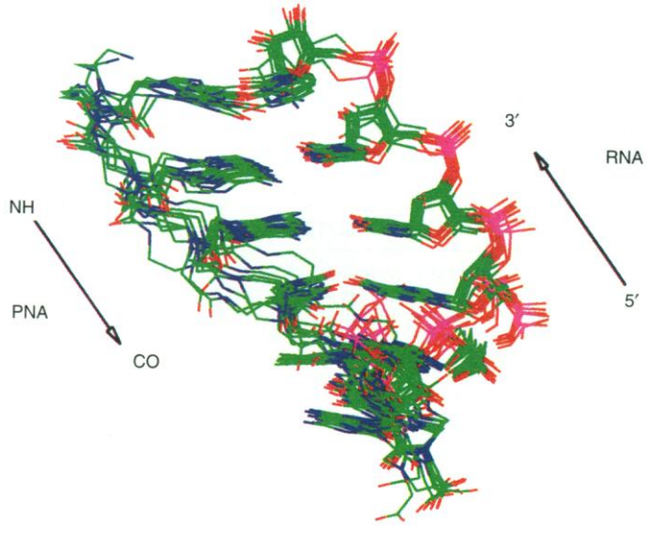

Fig. 4. Ten refined structures superimposed, with strand directionalities indicated. The average root-mean-square deviations for individual structures from the overall average structure are as follows: all atoms, 0.84 Å; PNA atoms, 0.97 Å; and RNA atoms, 0.68 Å. The root-mean-square deviation between the Arnott ideal structure for A form RNA (*13*) and the average RNA structure in the PNA-RNA heteroduplex is 1.13 Å.

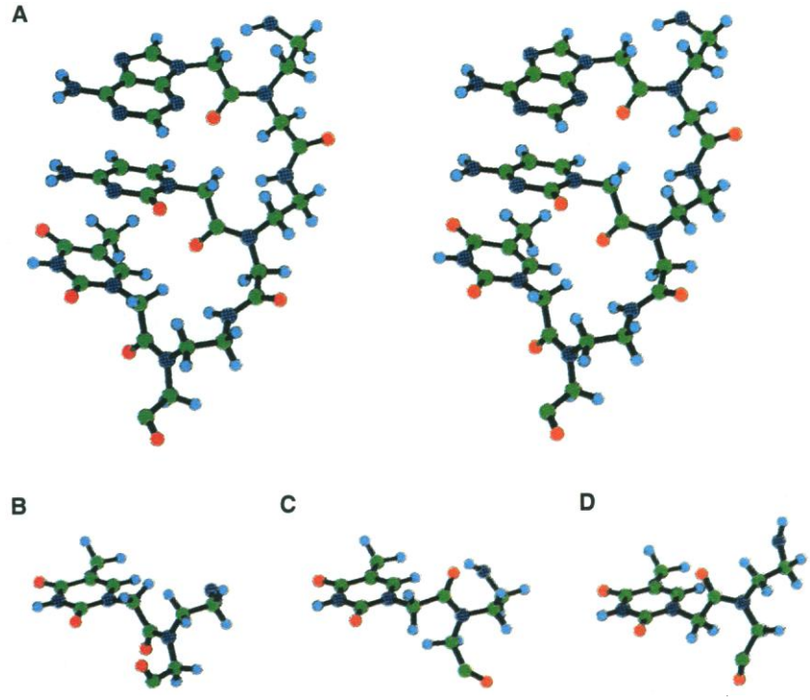

Fig. 5. (**A**) Stereo image of the average structure obtained from the incorporation of NMR restraints for the A_3–C_4–T_5 segment of the PNA strand. (**B** to **D**) Low-energy conformations of PNA suitable for antiparallel duplex formation (*15*).

tion of an "A" form conformation puts the PNA C7′ carbonyl group in a position isosteric to an RNA C2′, facilitating maximal solvent exposure of the two backbone carbonyl oxygens. The C7′ carbonyl oxygen is also placed proximal to H6 or H8 of the following base, allowing a favorable interaction between aromatic proton and carbonyl oxygen observed in several protein structures. The preferred ethylenediamine *gauche*$^+$ torsion permits the PNA strand to twist right-handed and maintain an interresidue backbone distance similar to that of RNA.

The NMR structures presented here provide a basis for the design of improved PNA-based antisense agents. PNA analogs stabilizing the ethylenediamine torsion (β) to *gauche*$^+$ or preforming the appropriate secondary amide rotamer (χ_1) could exhibit increased affinity, provided no unfavorable electrostatic, steric, or solvation interactions were introduced.

REFERENCES AND NOTES

1. P. C. Zamecnik and M. L. Stephenson, *Proc. Natl. Acad. Sci. U.S.A.* **75**, 280 (1978); M. L. Stephenson and P. C. Zamecnik, *ibid.*, p. 285.
2. J. S. Cohen, Ed., *Oligodeoxynucleotides: Antisense Inhibitors of Gene Expression* (Macmillan, Bethesda, MD, 1989); O. Pines and M. Inouye, *Trends Genet.* **1986**, 284 (1986).
3. E. Uhlmann and A. Peyman, *Chem. Rev.* **90** (no. 4), 544 (1990); J. F. Milligan, M. D. Matteucci, J. C. Martin, *J. Med. Chem.* **36**, 1923 (1993).
4. C. A. Stein and Y.-C. Cheng, *Science* **261**, 1004 (1993).
5. P. E. Nielsen, M. Egholm, R. H. Berg, O. Buchardt, *ibid.* **254**, 1497 (1991); O. Buchardt, M. Egholm, R. H. Berg, P. E. Nielsen, *Trends Biotechnol.* **11**, 384 (1993); M. Egholm, O. Buchardt, P. E. Nielsen, R. H. Berg, *J. Am. Chem. Soc.* **114**, 1895 (1992); M. Egholm, P. E. Nielsen, O. Buchardt, R. H. Berg, *ibid.*, p. 114.
6. M. Egholm *et al.*, *Nature* **365**, 566 (1993); J. C. Hanvey *et al.*, *Science* **258**, 1481 (1992); P. E. Nielsen, M. Egholm, R. H. Berg, O. Buchardt, *Nucleic Acids Res.* **21**, 197 (1993); N. J. Peffer *et al.*, *Proc. Natl. Acad. Sci. U.S.A.* **90**, 10648 (1993).
7. The compound [1,2-^{13}C,^{15}N]-glycine (Cambridge Isotopes, Woburn, MA) was converted to *N*-(*tert*-butoxycarbonyl)glycinal by the lithium ammonium hydride reduction of the Weinreb amide [J. A. Fehrentz and B. Castro, *Synthesis* **1983**, 676 (1983)]. Reductive amination [T. M. Zydowsky, J. F. Dellaria, H. N. Nellans, *J. Org. Chem.* **53**, 5607 (1988)] of *N*-(*tert*-butoxycarbonyl)glycinal with labeled methyl glycinate yielded the [^{13}C,^{15}N]-labeled backbone. The compound 1-Carboxymethylthymine was prepared as reported [A. S. Jones, P. Lewis, S. F. Withers, *Tetrahedron* **29**, 2293 (1973)] with [1,2-^{13}C] bromoacetic acid (Cambridge Isotopes) and coupled to the backbone under standard conditions. Amino protecting groups were changed to fluorenyl Methoxycarbonyl, and conversion to the pentafluorophenyl ester gave the activated monomer. The hexamer was prepared through solid-phase synthesis (S. A. Thomson *et al.*, unpublished results), converted to the *bis*-succinate derivative, purified by reverse-phase high-performance liquid chromatography, and characterized by electrospray. RNA was supplied by IDT (Coralville, IA) and characterized by capillary zone electrophoresis electrospray.
8. HMQC [A. Bax, R. H. Griffey, B. L. Hawkins, *J. Magn. Reson.* **55**, 81 (1983)]; 1,2D-X filtered NOE (G. Otting, H. Senn, G. Wagner, K. Wüthrich, *ibid.* **70**, 500 (1986)]; and heteronuclear Hartman Hahn [G. W. Kellogg, *ibid.* **98**, 176 (1992)] experiments were done in a similar way to homonuclear experiments (*9*), except that only 50 to 128 complex t_1 points were acquired with time proportional phase incrementation states.
9. TOCSY [A. Bax and D. G. Davis, *ibid.* **65**, 355 (1985)], 2Q [G. Wagner and E. R. P. Zuiderweg, *Biochem. Biophys. Res. Commun.* **113**, 854 (1983)], jump-return-NOESY [V. Sklenar, R. Tschudin, A. Bax, *J. Magn. Reson.* **75**, 352 (1987)], and NOESY [A. Kumar, R. R. Ernst, K. Wüthrich, *Biochem. Biophys. Res. Commun.* **95**, 1 (1980)] experiments were done at various mixing times with 800 μM complex in 20 mM $NaPO_4$, 50 mM NaCl, 0.25 mM EDTA (pH 7.4) at 10° to 25°C in H_2O or ^2H_2O. Generally, 2000 × 512 complex data points were acquired on a Bruker AMX-600 or AMX-500 (Rheinstetten, Germany) in the TPPI mode and transformed by the appropriate window functions and baseline corrections with FELIX version 2.1; Biosym, San Diego, CA) to yield 2000 × 2000 real matrices.
10. K. Wüthrich, *NMR of Proteins and Nucleic Acids* (Wiley Interscience, New York, 1986); G. Varani and I. Tinoco Jr., *Q. Rev. Biophys.* **24**, 479 (1991).
11. A. Bax, in *Methods of Enzymology*, N. J. Oppenheimer and T. L. James, Eds. (Academic Press, New York, 1989), vol. 176, pp. 164–167.
12. NOE cross-peak volumes were calculated from 2D NOESY data acquired at mixing time, τ_m, of 50, 100, and 200 ms with the FELIX utility. Buildup curves were generated, and cross-peak volumes were classed as strong ($1.8 < r_{ij} < 2.5$), medium ($2.5 < r_{ij} < 3.5$), or weak ($3.5 < r_{ij} < 5.0$) with the two-spin approximation as compared to peak volumes between protons having conformationally independent distances. Of 140 nontrivial interproton distances measured, 18 were interstrand, 65 were intrastrand sequential, and 66 were intraresidue. The 15 Watson-Crick hydrogen bonds were defined explicitly. Models of the PNA-RNA complex were built, randomly embedded with the experimental restraints, and refined with DSPACE (version 2.1; Hare Research, Bothell, WA). Ten structures were generated independently; all of which had fewer than residual violations >0.1 Å and good geometries. These structures were then refined with simulated annealing protocols in the program X-PLOR [A. T. Brunger, *X-PLOR (version 3.1) Manual* (Yale University, New Haven, CT, (1992)]. DSPACE structures were heated to 2000°K with only base pairing restraints. NMR restraints were gradually introduced, followed by slow cooling. These steps were repeated at 1000 K and 500 K, and the structures were then subjected to 200 steps of conjugate gradient-energy minimization. The AMBER potential-energy force field [S. J. Weiner, P. A. Kollman, D. T. Nguyen, D. A. Case, *J. Comp. Chem.* **7**, 230 (1986)] was used throughout the refinement. Atomic coordinates have been deposited in the Brookhaven Protein Data Bank.
13. R. Chandrasekaran and S. Arnott, in *Landolt-Bornstein, Nucleic Acids*, W. Saenger, Ed. (Springer-Verlag, Berlin, 1989), vol. VII/1b, p. 55.
14. O. Almarsson, T. C. Bruice, J. Kerr, R. N. Zuckermann, *Proc. Natl. Acad. Sci. U.S.A.* **90**, 7518 (1993); O. Almarsson and T. C. Bruice, *ibid.*, p. 9542.
15. A single thymine PNA monomer was subjected to a high-temperature (1100 K) molecular dynamics simulation by the program X-PLOR using the AMBER potential-energy force field (*12*). During the 100-ps simulation, structures were saved at 0.05-ps intervals. These structures were subsequently clustered and screened for conformers with distances and orientations from the NH_2^- terminus to the COOH-terminus to base N1 compatible with a standard A form RNA structure (*13*). Torsional parameters for these conformers were then used as guides in building distinct A-form RNA-PNA hexamer duplexes. The structures in Fig. 5, A to C were single monomers from these duplexes.

16. We thank M. Furth, P. W. Jeffs, M. H. Lambert, and B. Lovejoy for reading the manuscript; R. Anderegg, J. M. Ding, and D. Rose for compound analyses; P. W. Jeffs for his persistent support; and P. M. Myers for assistance.

28 February 1994; accepted 13 June 1994